Petrov-Galerkin Immersed Finite Element Method for Darcy/Darcy-Forchheimer Flow in Fractured Porous Media

Jijing Zhao and Shuyu Sun*[0000−0002−3078−864X]

School of Mathematical Sciences, Tongji University, Shanghai, China
suns@tongji.edu.cn(Shuyu Sun); 24310052@tongji.edu.cn(Jijing Zhao)

Abstract. This paper presents a Petrov-Galerkin immersed finite element method for coupled Darcy and Darcy-Forchheimer flows in fractured porous media. The matrix follows Darcy's law, while fractures are governed by the nonlinear Darcy-Forchheimer law to capture inertial effects. Fractures are treated as lower-dimensional interfaces embedded in the matrix, leading to an elliptic interface problem with multiple coupling conditions. The discrete method does not require mesh matching between the matrix and fracture. Instead, interface conditions are built into local basis functions on elements cut by fractures. This allows the immersed finite element space to capture both continuous and discontinuous pressure across fractures, making it applicable to both conductive and blocking fractures. Numerical examples and benchmarks demonstrate the proposed method on nonconforming meshes.

Keywords: Darcy/Darcy-Forchheimer Flow · Fractured porous media · Nonconforming meshes · Petrov-Galerkin immersed finite element method.

1 Introduction

Fluid flow in fractured porous media is involved in many earth science applications, including oil reservoir simulation, groundwater management, and geological disposal of nuclear waste. The presence of fractures introduces complexity to flow behavior. The difference between matrix and fracture permeability leads to different conductivity, which affects fluid flow in fractured porous media. When fractures are more permeable than the surrounding matrix, they act as preferential flow paths. Conversely, fractures with lower permeability can impede flow and cause pressure discontinuities across them. Accurate numerical simulation must therefore account for these effects.

In many practical situations, flow velocities in fractures can become high that inertial effects become non-negligible. While Darcy's law is commonly used to describe slow viscous flow in porous matrix, fracture flow may exhibit non-Darcian behavior due to inertial effects. In such cases, the nonlinear Darcy–Forchheimer law is more appropriate, as it incorporates additional pressure losses induced by inertial effects. The present work therefore considers a coupled system where

ICCS Camera Ready Version 2026
To cite this paper please use the final published version:
DOI: 10.1007/978-3-032-29918-5_9

matrix flow follows Darcy's law while fracture flow is governed by the Darcy-Forchheimer law.

The discrete fracture model (DFM), also referred to as the mixed-dimensional fracture model, treats fractures as lower-dimensional interfaces embedded in the matrix. This dimension reduction avoids refining the mesh around fractures and improves computational efficiency while preserving accuracy. As a result, DFM has been widely adopted [1–3, 9]. Conventional DFM requires the fracture mesh to align with the matrix mesh. To overcome the conforming mesh constraint, several methods have been developed that allow nonconforming (unfitted) grids. The embedded discrete fracture model (EDFM) [4] is one such approach. It retains explicit fracture representation while relaxing mesh alignment. Li and Lee [4] introduced EDFM for black oil models, and subsequent work by Moinfar et al. [5, 6] extended its application. The extended finite element method (XFEM) offers another mesh-independent approach. Originally developed for elliptic interface problems [7], XFEM was later adapted for hybrid-dimensional fracture models [8]. Additional degrees of freedom and enrichment functions are introduced in elements around fractures to capture their geometric and physical features [10–12]. This fully decouples fracture and matrix meshes.Yang et al. [13] described fractured media using a mixed-dimensional model with a Dirac delta function in the permeability tensor and applied the Galerkin method on nonconforming grids. This approach reduces computation time while maintaining accuracy, but it initially assumed continuous pressure across fractures and could not handle blocking fractures effectively. Subsequent extensions [14, 15] addressed this limitation. Other unfitted methods, such as the cut finite element method [17] and Lagrange multiplier methods [16], have also been explored.

In this work, we develop a Petrov-Galerkin immersed interface finite element method for the mixed-dimensional fracture model with coupled Darcy and Darcy-Forchheimer flows. The key idea is to embed fracture interface conditions into the local basis functions of elements intersected by fractures, allowing matrix and fracture meshes to be nonconforming.

The immersed finite element method originated from Li et al. [18] for one-dimensional interface problems and has since been extended to higher-order approximations [19, 20], two-dimensional [21–23], and three-dimensional elliptic interface problems [24–26]. Classical immersed finite element methods [21] face consistency issues because the basis functions do not lie in H1, which can affect convergence. Adding penalty terms at element boundaries [22] helps restore consistency. Alternatively, the Petrov-Galerkin formulation uses standard finite element functions as test functions while keeping immersed basis functions for the trial space, ensuring consistency without additional penalties. The Petrov-Galerkin immersed finite element method has seen rapid development for elliptic interface problems in two [27, 28, 31] and three dimensions [29, 30]. However, existing work typically assumes interface jumps that are either homogeneous or given as explicit functions. This differs from the fracture model [9], where interface conditions arise from coupling unknowns in different subdomains. In our approach, the trial space uses immersed basis functions that

ICCS Camera Ready Version 2026
To cite this paper please use the final published version:
DOI: 10.1007/978-3-032-29918-5_9

incorporate fracture-matrix interactions, while the test space consists of standard conforming finite element functions. The fracture is treated as an interface with Robin-type coupling conditions, which are built directly into the local basis functions on cut elements. Unlike traditional immersed interface finite element method, our method introduces explicit degrees of freedom on fractures, and the immersed basis functions are coupled with these fracture unknowns. A preliminary of this work, focusing on the Darcy-Darcy coupled system, was published in [35]. The present paper extends the formulation to incorporate the nonlinear Darcy-Forchheimer flow in fractures. The proposed scheme offers several features. First, it eliminates the need for conforming meshes. Second, it captures both continuous and discontinuous pressure across fractures, making it applicable to conductive and blocking fractures. Third, the formulation is straightforward, requiring no penalty terms. Meanwhile, this method also has some limitations. In particular, small-angle cuts or multiple fractures within a single element may lead to ill-conditioned linear systems, and stabilization or preconditioning techniques are often required to ensure numerical stability.

In Section 2, we present the mixed-dimensional Darcy and Darcy-Forchheimer flows and their discretization on non-conforming meshes. In Section 3, we verify the convergence order of the scheme on nonconforming meshes and validate it with two benchmark tests.

2 The problem and discretization

2.1 Mixed-dimensional Darcy/Darcy-Forchheimer fracture model

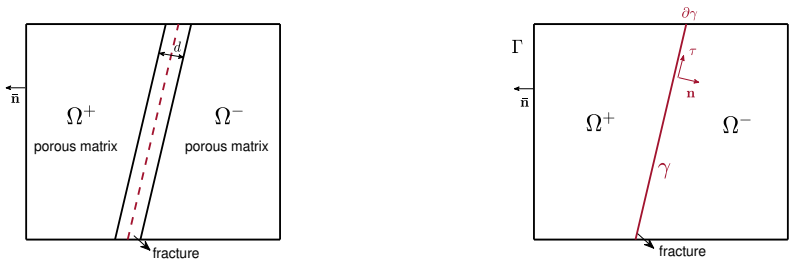

Fig. 1. Left: equi-dimensional fracture; Right: mixed-dimensional fracture.

We suppose that Ω is a convex domain in R^2, with its boundary $\partial\Omega = \partial_D\Omega \cup \partial_N\Omega$, $\partial_D\Omega \cap \partial_N\Omega = \emptyset$. Let $\bar{\mathbf{n}}$ be the outward unit normal vector on $\partial\Omega$. For mixed-dimensional fracture, the hyperplane γ divides the porous matrix into two part Ω^+ and Ω^-, see right of Fig. 1. We denote by $\Omega_m = \Omega^+ \cup \Omega^-$ the porous matrix in fractured porous media, while the γ represents the fracture. Obviously, $\Omega = \Omega_m \cup \gamma$. Let $\mathbf{n}$ be the unit normal vector on γ oriented from Ω^+ to Ω^-. The outward unite normal to $\partial\Omega^+$ on γ is then $\mathbf{n}^+ = \mathbf{n}$, and the

ICCS Camera Ready Version 2026
To cite this paper please use the final published version:
DOI: 10.1007/978-3-032-29918-5_9

outward unit normal to $\partial\Omega^-$ is $\mathbf{n}^- = -\mathbf{n}$. Let τ be a unit tangential vector on γ so that $(\tau, \mathbf{n})$ is positively oriented. In the mixed-dimensional model, $\Gamma = (\partial\Omega^+ \cap \partial\Omega) \cup (\partial\Omega^- \cap \partial\Omega)$ is defined as the boundary of the porous matrix, while $\partial\gamma$ is the boundary of fracture. We suppose K is the hydraulic conductivity (or permeability tensor), Q a source term. We assume that there exists positive constants $K_{\min}$ and $K_{\max}$ such that $K_{\min} \leqslant K(x) \leqslant K_{\max}, \forall x \in \Omega$.

Let us define K_γ as the diagonal permeability tensor restricted to the fracture. Additionally, let K_γ^τ and $K_\gamma^{\mathbf{n}}$ represent the tangential and normal permeabilities, respectively. $\nabla_\tau \cdot$ and ∇_τ are defined as tangential divergence and tangential gradient along the fracture. The average and jump operators are denoted as

$$\{q\} := \left(\frac{q^+ + q^-}{2}\right)\Big|_\gamma, \qquad [\![q]\!] := \left(q^+ - q^-\right)|_\gamma.$$

We consider the following problem, which was derived in [34, 33]:

$$\begin{aligned} \mathbf{u} + K\nabla p &= 0, \quad \text{in } \Omega_m, \\ \operatorname{div} \mathbf{u} &= Q, \quad \text{in } \Omega_m, \\ p &= p_d, \quad \text{on } \Gamma. \end{aligned} \tag{1}$$

Together with the Darcy-Forchheimer flow in fracture:

$$\begin{aligned} (1 + \frac{\beta}{d}|\mathbf{u}_\gamma|)\mathbf{u}_\gamma &= -K_\gamma^\tau d \nabla_\tau p_\gamma, \quad \text{on } \gamma, \\ \operatorname{div}_\tau \mathbf{u}_\gamma &= Q_\gamma + [\![\mathbf{u}\cdot\mathbf{n}]\!], \quad \text{on } \gamma, \\ p_\gamma &= p_{d,\gamma}, \quad \text{on } \partial\gamma. \end{aligned} \tag{2}$$

The interface condition that coupling Darcy and Darcy-Forchheimer flow on fracture is

$$\begin{aligned} [\![p]\!] &= 2\kappa\{-K\nabla p \cdot \mathbf{n}\}, \\ [\![-K\nabla p \cdot \mathbf{n}]\!] &= \frac{2}{2\xi - 1}\frac{1}{\kappa}(\{p\} - p_\gamma), \end{aligned} \tag{3}$$

where $\mathbf{n}$ is the unit normal vector on γ, directed outward from Ω_+, d is fracture width, $\kappa = d(2K_\gamma^n)^{-1}$ is a coefficient function on γ related directly to the fracture width and inversely to the normal component of the permeability of the physical fracture, the parameter ξ is a constant greater than $1/2$. The coefficient β is the Forchheimer coefficient on γ, assumed to be scalar.

Assuming that the Forchheimer coefficient is scale, we have

$$\frac{\beta}{d}|\mathbf{u}_\gamma|^2 + |\mathbf{u}_\gamma| - |K_\gamma^\tau d \nabla_\tau p_\gamma| = 0.$$

Dropping the negative term, we get $|\mathbf{u}_\gamma|$,

$$|\mathbf{u}_\gamma| = \frac{-1 + \sqrt{1 + 4\frac{\beta}{d}|K_\gamma^\tau d \nabla_\tau p_\gamma|}}{2\frac{\beta}{d}}.$$

ICCS Camera Ready Version 2026
To cite this paper please use the final published version:
DOI: 10.1007/978-3-032-29918-5_9

Then the flux $\mathbf{u}_\gamma$ can then be written as follows

$$\mathbf{u}_\gamma = -\frac{2K_\gamma^\tau d\nabla_\tau p_\gamma}{1+\sqrt{1+4\frac{\beta}{d}|K_\gamma^\tau d\nabla_\tau p_\gamma|}}. \tag{4}$$

2.2 Weak formulation of the model problem and discretization

We use the standard notations for the Sobolev spaces. Let

$$H_0^1(\Omega_m) = \{p = (p^+, p^-) : p^+ \in H^1(\Omega^+), p^- \in H^1(\Omega^-), p|_\Gamma = 0\},$$
$$H_0^1(\gamma) = \{p_\gamma : p_\gamma \in H^1(\gamma), p_\gamma|_{\partial\gamma} = 0\}.$$

Transpose the velocity equation into the mass conservation equation, and then multiply $q \in H_0^1(\Omega_m)$ and $q_f \in H_0^1(\gamma)$ on both sides of pressure equation in porous matrix and fracture respectively. And then integrating over the corresponding subdomains, we can deduce the following weak formulation by the Green formulation and the interface conditions (3). Find $(p, p_\gamma) \in H_0^1(\Omega_m) \times H_0^1(\gamma)$ such that for all $(q, q_\gamma) \in H_0^1(\Omega_m) \times H_0^1(\gamma)$,

$$\mathcal{A}_m(p,q) + \mathcal{A}_\gamma(p_\gamma, q_\gamma) + \mathcal{I}((p,p_\gamma),(q,q_\gamma)) = \mathcal{L}(q,q_\gamma), \tag{5}$$

where the multilinear forms are defined as

$$\mathcal{A}_m(p,q) = \int_{\Omega^+} K\nabla p^+ \cdot \nabla q^+ + \int_{\Omega^-} K\nabla p^- \cdot \nabla q^-,$$
$$\mathcal{A}_\gamma(p_\gamma, q_\gamma) = \int_\gamma \frac{2K_\gamma^\tau d}{1+\sqrt{1+4\frac{\beta}{d}|K_\gamma^\tau d\nabla_\tau p_\gamma|}}\nabla_\tau p_\gamma \cdot \nabla_\tau q_\gamma,$$
$$\mathcal{I}((p,p_\gamma),(q,q_\gamma)) = \int_\gamma \frac{1}{2\kappa}[\![p]\!]\cdot[\![q]\!] + \int_\gamma \frac{2}{2\xi-1}\frac{1}{\kappa}\left(\{p\}-p_\gamma\right)\left(\{q\}-q_\gamma\right),$$
$$\mathcal{L}(q,q_\gamma) = \int_{\Omega_m} Qq + \int_\gamma dQ_\gamma q_\gamma.$$

Now we turn to the finite dimensional discretization. Let $\mathcal{T}_h$ be the finite element partition of region Ω_m consisting of triangular or rectangular elements T. Denote by $\mathcal{T}_h^\gamma$ the partition of $(n-1)$-dimensional fracture and made up of elements F. Elements in $\mathcal{T}_h$ can be categorized into two classes: interface elements whose interior is cut through by fracture γ and regular elements that either has no intersection with fractures or $\gamma \cap T \subset \partial T$. In order to define the interface elements well, we also need to assume that interface end points are enforced to be on the edges of its element. Denote the set of all interface elements by $\mathcal{T}_h^i$, and the set of regular elements by $\mathcal{T}_h^r$. And naturally $\mathcal{T}_h = \mathcal{T}_h^i \cup \mathcal{T}_h^r$. We also denote ε_h^b as the sets of boundary edges in Γ.

For approximating pressure in fracture, we define

$$V_h^\gamma = \{q_f \in H^1(\gamma) : q_f|_F \in P_1(F), q_f|_{\partial\gamma\cap F} = 0, \forall F \in \mathcal{T}_h^\gamma\}.$$

ICCS Camera Ready Version 2026
To cite this paper please use the final published version:
DOI: 10.1007/978-3-032-29918-5_9

Meanwhile, the standard conforming bilinear (or linear) space for porous matrix is defined as

$$V_h^L = \{q \in H^1(\Omega_m) : q|_T \in Q_1(T)(\text{or } P_1(T)), q|_{\Gamma\cap T} = 0, \forall T \in \mathcal{T}_h\}.$$

We then denote by V_h^{IFE} the IFE space, which includes all functions such that:

1 For $T \in \mathcal{T}_h^i$, the local function $p_h|_T$ need to be divided into piecewise polynomials, which satisfy the interface conditions (3) and the continuity at each element vertices.
2 For $T \in \mathcal{T}_h^r$, the standard construction is adopted for basis functions.

After considering the boundary condition, the subspace of V_h^{IFE} space is

$$V_{h,0}^{IFE} = \{q : q \in V_h^{IFE}, q|_e = 0, \forall e \in \varepsilon_h^b\}.$$

We have elaborate on the construction of local functions in the interface element of $\mathcal{T}_h^i$ in [35]. Then our scheme based on PG-IFE for hybrid-dimensional fracture problem is to find $(p_h, p_{f,h}) \in V_h^{IFE} \times V_h^{\gamma}$ such that

$$\int_{\Omega_m} K\nabla_h p_h \cdot \nabla q + \int_{\gamma} \alpha_{\gamma}^{\xi} \left(\{p_h\} - p_{\gamma,h}\right)\left(\{q\} - q_{\gamma}\right) \tag{6}$$

$$+ \int_{\gamma} \frac{2K_{\gamma}^{\tau} d}{1 + \sqrt{1 + 4\frac{\beta}{d}|K_{\gamma}^{\tau} d \nabla_{\tau} p_{\gamma,h}|}} \nabla_{\tau} p_{\gamma,h} \cdot \nabla_{\tau} q_{\gamma} = \mathcal{L}(q, q_{\gamma}), \tag{7}$$

for $(q, q_{\gamma}) \in V_h^L \times V_h^{\gamma}$, where

$$\mathcal{L}(q, q_{\gamma}) = \int_{\Omega_m} Q(x) q + \int_{\gamma} dQ_{\gamma}(x) q_{\gamma}.$$

And ∇_h is the discrete gradient operator defined on each subregion in interface element.

Our proposed scheme is simpler than the weak form (5), as it removes the term $\int_{\gamma} \alpha_{\gamma} [\![p_h]\!] \cdot [\![q]\!]$. This is because our test function space uses the standard basis function space, and its jump is 0 on the interface.

For the Darcy/Darcy–Forchheimer fracture model, the nonlinearity appears in the fracture region, while the matrix domain is governed by the linear Darcy equation. Therefore, in the iterative procedure, only the fracture region needs to be updated, and the matrix part remains linear at each iteration. The iteration is terminated when the difference between two successive fracture pressures satisfies $\|p_{\gamma,i} - p_{\gamma,i-1}\| \leq \text{tol}$, where tol is a prescribed tolerance.

3 Numerical examples

In this section, we present numerical experiments to validate our proposed method. These experiments include convergence tests and benchmarks that cover two fractures distributions. This nonlinear problem is solved by an iterative method, and the tolerance is uniformly set to 10^{-6}.

ICCS Camera Ready Version 2026
To cite this paper please use the final published version:
DOI: 10.1007/978-3-032-29918-5_9

3.1 Convergence test

For the error between exact solution and numerical solution, in the later tables, we set

$$\|e\|_{L^\infty(\Omega_m)} = \max_{T\in\mathcal{T}_h}\|p-p^h\|_{L^2(T)}, \quad \|e\|_{0,\Omega_m} = \left(\sum_{T\in\mathcal{T}_h}\|p-p^h\|^2_{L^2(T)}\right)^{1/2},$$

$$\|e\|_{1,\Omega_m} = \left(\sum_{T\in\mathcal{T}_h}\|\nabla(p-p^h)\|^2_{L^2(T)}\right)^{1/2}, \quad \|e_f\|_{L^\infty(\gamma)} = \max_{F\in\mathcal{T}_h^\gamma}\|p_f-p_f^h\|_{L^2(F)},$$

$$\|e_f\|_{0,\gamma} = \left(\sum_{F\in\mathcal{T}_h^\gamma}\|p_f-p_f^h\|^2_{L^2(F)}\right)^{1/2}, \quad \|e_f\|_{1,\gamma} = \left(\sum_{F\in\mathcal{T}_h^\gamma}\|\nabla(p_f-p_f^h)\|^2_{L^2(F)}\right)^{1/2}.$$

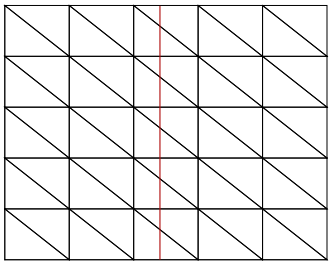

Fig. 2. The triangular nonconforming mesh.

Example 1. Consider the model in domains $\Omega^+ = [0, 0.5) \times [0, 1], \Omega^- = (0.5, 1] \times [0, 1]$ and $\gamma = \{x = 0.5\} \times [0, 1]$. The right-hand side functions and boundary condition are determined according to the following analytic solution

$$\begin{cases} p^+ = sin(2\pi x)sin(2\pi y), & \text{in } \Omega^+, \\ p^- = (x-1)sin(2\pi y), & \text{in } \Omega^-, \\ p_f = -(\frac{1}{4} + \frac{2\pi+1}{16\pi-8})sin(2\pi y), & \text{in } \gamma, \end{cases} \tag{8}$$

with permeability tensor $K = \mathbf{I}$, $K_\gamma = \begin{pmatrix} 10^{-2}\times(2\pi-1), & 0 \\ 0, & 100 \end{pmatrix}$, $\xi = \frac{3}{4}$, $\beta = 0.01$ and the fracture width $d = 0.01$, parameter $\kappa = \frac{1}{2(2\pi-1)}$.

In this experiment, we can observe the discontinuity of the pressure field at the interface $x = 0.5$. The computed errors and convergence rates for the

ICCS Camera Ready Version 2026
To cite this paper please use the final published version:
DOI: 10.1007/978-3-032-29918-5_9

Table 1. Results of Example 1 on triangular mesh.

N	$\|e\|_{L^\infty(\Omega_m)}$	rate	$\|e\|_{0,\Omega_m}$	rate	$\|e\|_{1,\Omega_m}$	rate	$\|e_f\|_{L^\infty(\gamma)}$	rate	$\|e_f\|_{0,\gamma}$	rate	$\|e_f\|_{1,\gamma}$	rate
5×5	1.60e-01		1.38e-01		1.87e+00		1.02e-01		4.97e-02		4.96e-01	
11×11	3.86e-02	1.80	3.61e-02	1.70	9.75e-01	0.82	3.11e-02	1.51	1.57e-02	1.46	1.89e-01	1.22
21×21	1.89e-02	1.11	1.13e-02	1.80	5.50e-01	0.88	1.22e-02	1.44	6.30e-03	1.41	9.26e-02	1.11
41×41	9.61e-03	1.01	3.61e-03	1.70	3.09e-01	0.86	5.09e-03	1.31	2.65e-03	1.29	4.59e-02	1.05
81×81	4.83e-03	1.01	1.30e-03	1.50	1.79e-01	0.80	2.26e-03	1.19	1.18e-03	1.18	2.29e-02	1.02
161×161	2.42e-03	1.01	5.40e-04	1.28	1.09e-01	0.72	1.06e-03	1.11	5.55e-04	1.10	1.14e-02	1.01
321×321	1.21e-03	1.00	2.47e-04	1.13	7.02e-02	0.64	5.09e-04	1.06	2.68e-04	1.05	5.71e-03	1.01

L^∞ norm, L^2 norm, and H^1 norm of the pressure in matrix and fracture are presented in Table 1. linear polynomial approximation on the triangular grid, as shown in Table 1, the convergence order is suboptimal, i.e., $O(h)$ in L^2 norm and L^∞ norm. However, this does not affect the convergence of the method.

3.2 Benchmarks

In this section, we consider two benchmark problems [9, 34] to validate the proposed method. Examples 2 and 3 are designed to verify the ability of the discrete formulation to handle immersed fractures. We assume that the mass transfer across the immersed tip can be neglected [32], i.e., we apply the Neumann boundary condition $(-K_\gamma^\tau \nabla_\tau p_f) \cdot \tau = 0$ on $\partial\gamma$. On the fracture boundary intersecting with the porous matrix boundary, we apply the same boundary condition as that applied on Γ.

Example 2. We consider a test case with a single through-going fracture [9], which intersects the top and bottom boundaries and divides the computational domain into two subdomains. The results obtained by our numerical method are compared with those produced by a locally refined method (see Fig. 4(a)).

In this example, the fracture permeability is assumed to be relatively large. We set $K = 10^{-9}\mathbf{I}$ for the matrix and $K_\gamma = 10^{-6}\mathbf{I}$ for the fracture. To facilitate comparison with the results reported in the literature, we take $\beta = 0$, which reduces the model to a coupled Darcy/Darcy fracture system. Also we take $\beta = 0.1$ for Darcy-Forchheimer test. The permeability configuration and the boundary conditions are shown in Fig. 3.

The equi-dimensional fracture model is computed on a locally refined mesh and used as the reference solution. Specifically, the fracture is treated as a two-dimensional region with $d = 0.01$, and local mesh refinement is applied in the fracture region, see Fig. 4(a). Figures 5–6 compare the reference solution with the numerical solution obtained by the nonconforming grid (Fig. 4(b)). The results indicate that the method is able to capture the conductive behavior of high-permeability fractures.

Example 3. In this example, we consider a cross-shaped fracture configuration formed by two intersecting fractures. Two different permeability regimes are examined: a conducting fracture with permeability tensor 10^8 and a blocking fracture with 10^{-8}. The matrix permeability tensor is set to $K = \mathbf{I}$. Homogeneous Neumann boundary conditions are imposed on the top and bottom boundaries

ICCS Camera Ready Version 2026
To cite this paper please use the final published version:
DOI: 10.1007/978-3-032-29918-5_9

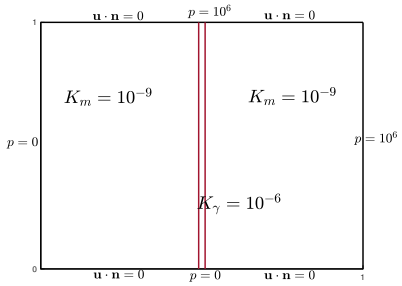

Fig. 3. Permeability and boundary conditions for Example 2.

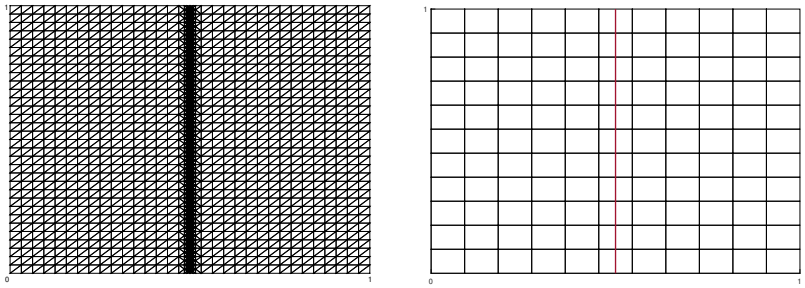

(a) Locally refined mesh. (b) Nonconforming mesh.

Fig. 4. Different meshes.

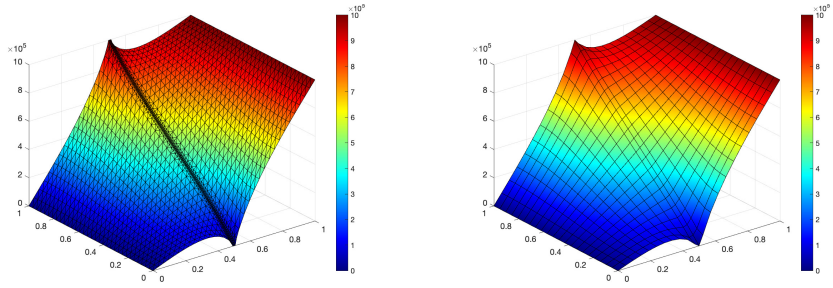

(a) The reference pressure solution on local refine mesh. (b) Numerical pressure solution on 21×21 nonconforming mesh.

Fig. 5. Solution by different meshes.

ICCS Camera Ready Version 2026
To cite this paper please use the final published version:
DOI: 10.1007/978-3-032-29918-5_9

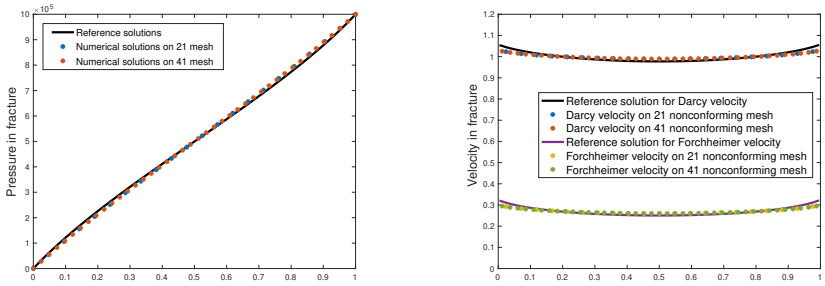

(a) The reference pressure solution on local refine mesh.

(b) Numerical pressure solution on 21×21 nonconforming mesh for $\beta = 0$ and 0.1.

Fig. 6. Comparison of numerical solutions in the fracture region.

of the computational domain, while Dirichlet conditions with pressures 1 and 0 are prescribed on the left and right boundaries, respectively. The two fractures are located at $\{x = 0.5,\ 0.25 \leqslant y \leqslant 0.75\}$ and $\{0.25 \leqslant x \leqslant 0.75,\ y = 0.5\}$, respectively. The remaining model parameters are taken as $\beta = 10$, $d = 0.01$, and $\xi = 3/4$.

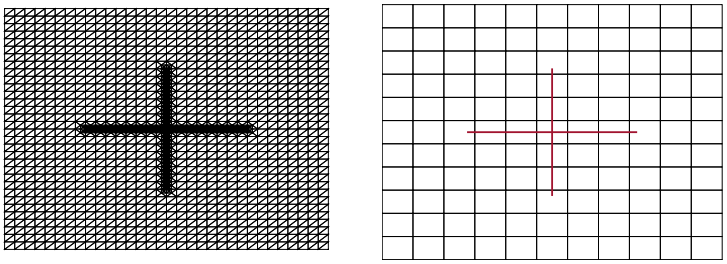

(a) Locally refined mesh.

(b) Nonconforming mesh.

Fig. 7. Meshes for Example 3.

In this example, we also compute the solution on a locally refined mesh as the reference solution, as shown in Fig. 7(a). The numerical solution obtained on our nonconforming mesh, shown in Fig. 7(b), is then compared with the reference solution. The results are shown in Figs. 8–10. The corresponding velocity fields are presented in Fig. 8(c) and 9(c). When the fracture permeability is high, the flow concentrates along the fractures. In contrast, when the fracture permeability is low, the fractures act as barriers, causing a pressure discontinuity, see Fig. 9(a)-(b). This behavior is also observed in Darcy/Darcy–Forchheimer fracture flow, due to the interface conditions. We present the numerical solutions on

ICCS Camera Ready Version 2026
To cite this paper please use the final published version:
DOI: 10.1007/978-3-032-29918-5_9

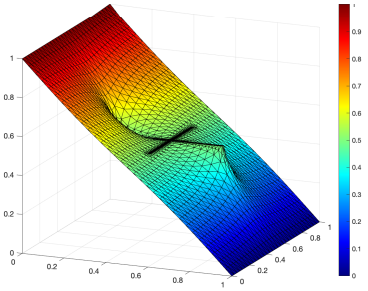

(a) Reference solutions on refined mesh.

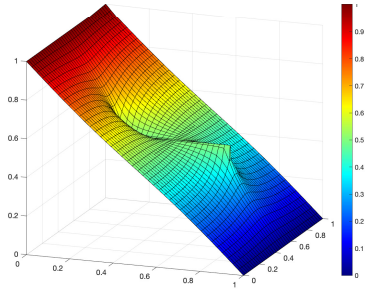

(b) Numerical solutions on nonconforming mesh.

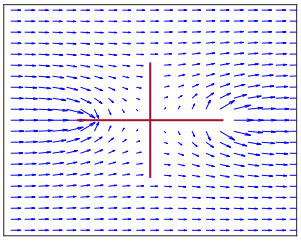

(c) Numerical velocity distribution.

Fig. 8. Pressure and velocity solutions for conductive fractures.

the fractures in Fig. 10. Here, fracture 1 denotes the fracture parallel to the x-axis. It can be observed that, due to the low normal conductivity of fracture 2, the fluid flow is blocked, which leads to a discontinuity in the solution. Our Petrov-Galerkin immersed method on nonconforming mesh is able to capture this discontinuity.

Although the proposed method works well in most cases, it still has some limitations. When multiple fractures(three or more fractures) intersect a single element, the treatment becomes more complicated. If these fractures are conductive, they can be approximated by a single equivalent fracture to simplify the implementation. In addition, if a fracture cuts through an element with a very small angle, the resulting system may become ill-conditioned, and additional preconditioning or stabilization techniques may be required.

4 Conclusions

This paper proposes a Petrov-Galerkin immersed finite element method for coupled Darcy and Darcy-Forchheimer flows in fractured porous media. The matrix obeys Darcy's law, while fractures follow the nonlinear Darcy-Forchheimer law to capture velocity inertial effects. Fractures are discretized on nonconforming meshes by embedding interface conditions into local basis functions, allowing independent mesh generation. The trial space uses immersed functions for

ICCS Camera Ready Version 2026
To cite this paper please use the final published version:
DOI: 10.1007/978-3-032-29918-5_9

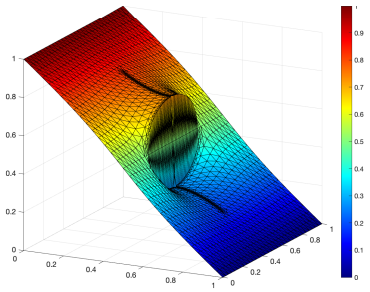

(a) Reference solutions on refined mesh.

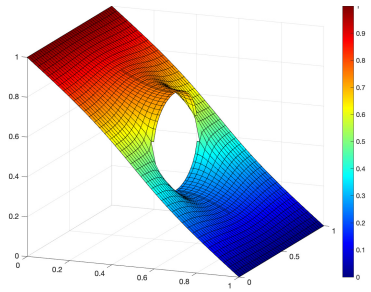

(b) Numerical solutions on nonconforming mesh.

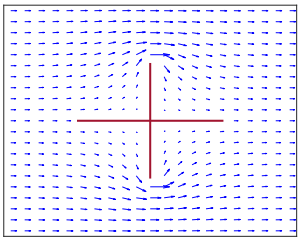

(c) Numerical velocity.

Fig. 9. Pressure and velocity solutions for blocking fractures.

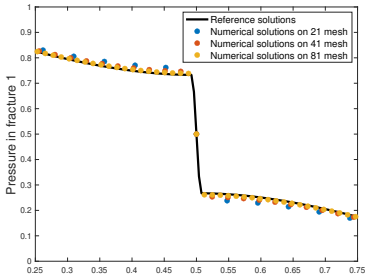

(a) Fracture 1.

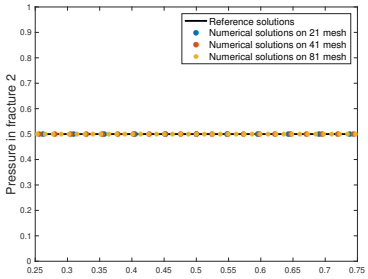

(b) Fracture 2.

Fig. 10. Compare pressure in different blocking fractures.

ICCS Camera Ready Version 2026
To cite this paper please use the final published version:
DOI: 10.1007/978-3-032-29918-5_9

fracture-matrix coupling, and the test space uses standard conforming functions. The method requires no penalty terms and handles both conductive and blocking fractures by enforcing pressure continuity or discontinuity. Numerical examples confirm its accuracy on nonconforming meshes.

Acknowledgments. The authors acknowledge the financial support from the National Key Research and Development Project of China (Grant No. 2023YFA1011701), the National Natural Science Foundation of China (Grant No. 12571466, 12501513), and the Fundamental Research Funds for the Central Universities. In addition, Shuyu Sun would like to express his gratitude for the support provided by the Shanghai Magnolia Talent Fund (Innovation Talent Category) of Shanghai Municipal Human Resources and Social Security Bureau and the Chang Jiang Scholars Program of the Ministry of Education of China. The work of J. Zhao was supported by the China Postdoctoral Science Foundation under Grant Number GZB20240552 and 2024M762396.

References

1. N. Schwenck, B. Flemisch, R. Helmig, B.I. Wohlmuth, 2015. Dimensionally reduced flow models in fractured porous media: crossings and boundaries. Comput. Geosci. 19, 1219–1230.
2. L. Formaggia, A. Fumagalli, A. Scotti, P. Ruffo, 2014. A reduced model for Darcy's problem in networks of fractures. ESAIM Math. Model. Numer. Anal. 48 (4), 1089–1116.
3. N. Frih, V. Martin, J.E. Roberts, A. Saada, Modeling fractures as interfaces with nonmatching grids, Comput. Geosci. 16 (4) (2012) 1043–1060.
4. L. Li, S.H. Lee, Efficient field-scale simulation of black oil in a naturally fractured reservoir through discrete fracture networks and homogenized media, SPE Reserv. Eval. Eng. 11(04) (2008) 750–758.
5. A. Moinfar, Development of an Efficient Embedded Discrete Fracture Model for 3D Compositional Reservoir Simulation in Fractured Reservoirs, 2013.
6. L.H. Odsæter, T. Kvamsdal, M.G. Larson, A simple embedded discrete fracture–matrix model for a coupled flow and transport problem in porous media, Comput. Methods Appl. Mech. Eng. 343 (2019) 572–601.
7. A. Hansbo, P. Hansbo, An unfitted finite element method, based on Nitsche's method, for elliptic interface problems, Comput. Methods Appl. Mech. Eng. 191(47–48) (2002) 5537–5552.
8. A. Fumagalli, A. Scotti, An efficient XFEM approximation of Darcy flows in arbitrarily fractured porous media, Oil Gas Sci. Technol. (Revue d'IFP Energies nouvelles) 69(4) (2014) 555–564.
9. V. Martin, J. Jaffré, J.E. Roberts, Modeling fractures and barriers as interfaces for flow in porous media, SIAM J. Sci. Comput. 26(5) (2005) 1667–1691.
10. S. Salimzadeh, N. Khalili, Fully coupled XFEM model for flow and deformation in fractured porous media with explicit fracture flow, Int. J. Geomech. 16(4) (2015) 04015091.
11. B. Flemisch, A. Fumagalli, A. Scotti, A review of the XFEM-based approximation of flow in fractured porous media, in: Advances in Discretization Methods, Springer, Cham, 2016, pp.47–76.

ICCS Camera Ready Version 2026
To cite this paper please use the final published version:
DOI: 10.1007/978-3-032-29918-5_9

12. C. D'Angelo, A. Scotti, A mixed finite element method for darcy flow in fractured porous media with non-matching grids. ESAIM: Math. Modell. Numer. Anal. 46 (2), (2012) 465–489.
13. Z. Xu, Y. Yang, The hybrid dimensional representation of permeability tensor: A reinterpretation of the discrete fracture model and its extension on nonconforming meshes. J. Comput. Phys. 415, (2019) 109523.
14. Z. Xu, Z. Huang, Y. Yang, The hybrid-dimensional Darcy's law: a nonconforming reinterpreted discrete fracture model (RDFM) for single-phase flow in fractured media. J. Comput. Phys. 473, (2023) 111749.
15. G. Fu, Y. Yang, A hybrid-mixed finite element method for single-phase Darcy flow in fractured porous media, Adv. Water Resour. 161 (2022) 104129.
16. M. Köppel, V. Martin, J. Jaffré, J.E. Roberts, A Lagrange multiplier method for a discrete fracture model for flow in porous media, Comput. Geosci. 23(2) (2019) 239–253.
17. E. Burman, P. Hansbo, M.G. Larson, K. Larsson, Cut finite elements for convection in fractured domains, Comput. Fluids 179 (2019) 726–734.
18. Z. Li, The immersed interface method using a finite element formulation, Appl. Numer. Math. 27 (3) (1998) 253–267.
19. S. Adjerid, T. Lin, A p-th degree immersed finite element for boundary value problems with discontinuous coefficients, Appl. Numer. Math. 59 (6) (2009) 1303–1321.
20. W. Cao, X. Zhang, Z. Zhang, Superconvergence of immersed finite element methods for interface problems, Adv. Comput. Math. 43 (4) (2017) 795–821.
21. Z. Li, T. Lin, X. Wu, New cartesian grid methods for interface problems using the finite element formulation, Numer. Math. 96 (1) (2003) 61–98.
22. T. Lin, Y. Lin, X. Zhang, Partially penalized immersed finite element methods for elliptic interface problems, SIAM J. Numer. Anal. 53 (2) (2015) 1121–1144.
23. J. Guzmán, M.A. Sánchez, M. Sarkis, On the accuracy of finite element approximations to a class of interface problems, Math. Comp. 85 (301) (2016) 2071–2098.
24. R. Kafafy, T. Lin, Y. Lin, J. Wang, Three-dimensional immersed finite element methods for electric field simulation in composite materials, Internat. J. Numer. Methods Engrg. 64 (7) (2005) 940–972.
25. R. Guo, T. Lin, An immersed finite element method for elliptic interface problems in three dimensions, J. Comput. Phys. 414 (1) (2020) 109478.
26. R. Guo, X. Zhang, Solving three-dimensional interface problems with immersed finite elements: A-priori error analysis, J. Comput. Phys. 441 (2021) 110445.
27. S. Hou, X.-D. Liu, A numerical method for solving variable coefficient elliptic equation with interfaces, J. Comput. Phys. 202 (2) (2005) 411–445.
28. L. Wang, S. Hou, L. Shi, P. Zhang, A bilinear Petrov–Galerkin finite element method for solving elliptic equation with discontinuous coefficients, Adv. Appl. Math. Mech. 11 (1) (2019) 216–240.
29. S. Hou, P. Song, L. Wang, H. Zhao, A weak formulation for solving elliptic interface problems without body fitted grid, J. Comput. Phys. 249 (2013) 80–95.
30. L. Wang, S. Hou, L. Shi, A numerical method for solving three-dimensional elliptic interface problems with triple junction points, Adv. Comput. Math. 44 (1) (2018) 175–193.
31. C. He, S. Zhang, X. Zhang, Error analysis of Petrov-Galerkin immersed finite element methods, Comput. Methods Appl. Mech. Engrg. 404 (2023) 115744.
32. P. Angot, F. Boyer, F. Hubert, 2009. Asymptotic and numerical modelling of flows in fractured porous media. ESAIM: M2AN 43, 239–275.

ICCS Camera Ready Version 2026
To cite this paper please use the final published version:
DOI: 10.1007/978-3-032-29918-5_9

33. P. Knabner and J. E. Roberts, Mathematical analysis of a discrete fracture model coupling Darcy flow in the matrix with Darcy-Forchheimer flow in the fracture, ESAIM: Mathematical Modelling and Numerical Analysis, vol. 48, no. 5, pp. 1451–1472, 2014.
34. N. Frih, J. E. Roberts, and A. Saada, Modeling fractures as interfaces: a model for Forchheimer fractures, Computational Geosciences, vol. 12, no. 1, pp. 91–104, 2008.
35. J. Zhao and H. Rui, A discrete fracture-matrix approach based on Petrov-Galerkin immersed finite element for fractured porous media flow on nonconforming mesh, J. Comput. Phys., vol. 499, p. 112718, 2024.

ICCS Camera Ready Version 2026
To cite this paper please use the final published version:
DOI: 10.1007/978-3-032-29918-5_9